Cell

Natively Unfolded Nucleoporins Gate Protein Diffusion across the Nuclear Pore Complex

Samir S. Patel,[1,2] Brian J. Belmont,[2] Joshua M. Sante,[2] and Michael F. Rexach[1,*]
[1] MCD Biology, University of California Santa Cruz, Santa Cruz, CA 95064, USA
[2] Biological Sciences, Stanford University, Stanford, CA 94305, USA
*Correspondence: rexach@biology.ucsc.edu
DOI 10.1016/j.cell.2007.01.044

SUMMARY

Nuclear pore complexes (NPCs) form aqueous conduits in the nuclear envelope and gate the diffusion of large proteins between the cytoplasm and nucleoplasm. NPC proteins (nucleoporins) that contain phenylalanine-glycine motifs in filamentous, natively unfolded domains (FG domains) line the diffusion conduit of the NPC, but their role in the size-selective barrier is unclear. We show that deletion of individual FG domains in yeast relaxes the NPC permeability barrier. At the molecular level, the FG domains of five nucleoporins anchored at the NPC center form a cohesive meshwork of filaments through hydrophobic interactions, which involve phenylalanines in FG motifs and are dispersed by aliphatic alcohols. In contrast, the FG domains of four peripherally anchored nucleoporins are generally noncohesive. The results support a two-gate model of NPC architecture featuring a central diffusion gate formed by a meshwork of cohesive FG nucleoporin filaments and a peripheral gate formed by repulsive FG nucleoporin filaments.

INTRODUCTION

The eukaryotic NPC is embedded in the nuclear envelope (Figure 1A) and serves as the sole aqueous conduit connecting the nucleoplasm and cytoplasm of cells (reviewed in Tran and Wente, 2006). It is composed of ~32 different proteins (nups), each present in multiple copies. The 13 FG nups contain Phe-Gly repeats interspersed along natively unfolded domains (Figure 1A). These 150–700 amino acid (aa) domains likely exist as flexible filaments throughout the NPC structure (Denning et al., 2003).

The role of FG nups in karyopherin-mediated transport of large proteins is well established, but it is less clear what role they play in the permeability barrier of the NPC, which keeps non-karyophilic proteins larger than 40 kDa from entering (or exiting) the nucleus by simple diffusion. Conceptually, the barrier must contain a diffusion conduit for small proteins (<40 kDa), must prevent nuclear entry of large non-karyophilic proteins, and must flex to allow transport complexes of various shapes and sizes to pass through.

S. cerevisiae cells lacking the non-FG nups Nup170 or Nup188 are more permissive to diffusion of large proteins into the nucleus (Shulga et al., 2000). In these cells, nucleoporins (FG and non-FG) are not properly anchored at the NPC, and their mislocalization is exacerbated by the addition of aliphatic alcohols such as hexanediol or ethanol, by low temperature (4°C), or by ATP depletion (Shulga and Goldfarb, 2003). In *A. nidulans*, a transient loss of FG and non-FG nups from the NPC during its cell cycle is accompanied by a concomitant, reversible opening of the NPC permeability barrier (De Souza et al., 2004). Thus, FG and non-FG nups may function as physical elements of a molecular sieve, or as regulators of the sieve.

The virtual-gate model (Figure 1B, left) proposes that FG nup filaments function as repulsive bristles that form an entropic barrier at the NPC entrance (Rout et al., 2000). Consistently, the FG domain of one human nup (Nup153, anchored at the nuclear basket) displays biophysical properties characteristic of entropic repulsion when probed by atomic-force microscopy (Lim et al., 2006). It is unknown whether other FG domains behave similarly.

The selective-phase model (Figure 1B, right) proposes that the NPC permeability barrier is formed by a meshwork of FG nup filaments interacting weakly via hydrophobic attraction between FG motifs (Ribbeck and Gorlich, 2001). Consistently, aliphatic alcohols that interfere with hydrophobic attractions disrupt the NPC permeability barrier in perforated cells (Ribbeck and Gorlich, 2002). Similarly, exposure of live yeast to alcohols weakens their NPC permeability barrier (Shulga and Goldfarb, 2003). Lastly, the FG domain of one yeast nup (Nsp1; anchored at the NPC center) forms homotypic interactions in vitro but only after exposure to extreme chemical environments (Frey et al., 2006).

In this study we analyzed 13 FG domains of *S. cerevisiae* nups, and we provide in vivo and in vitro evidence that

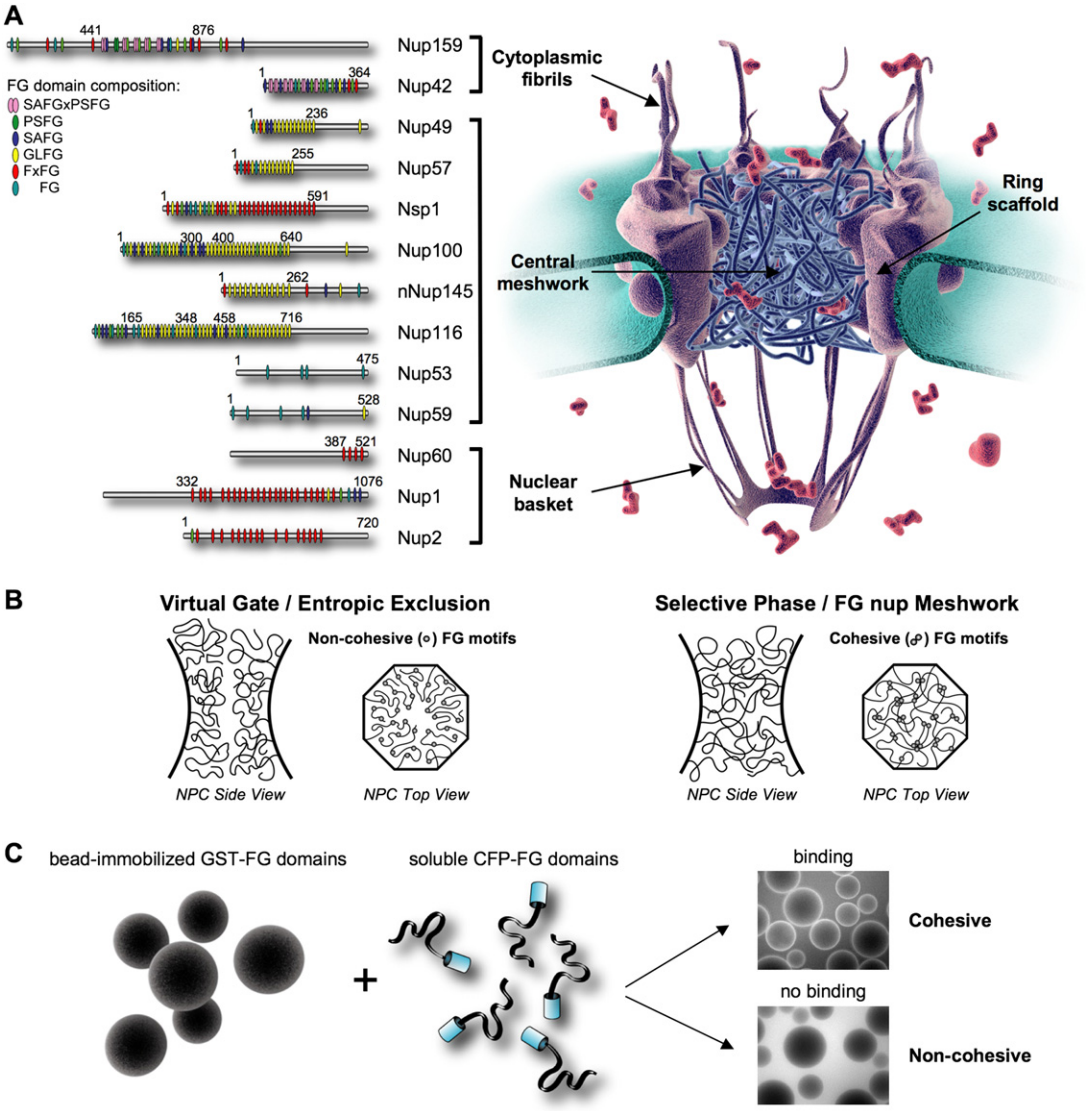

Figure 1. Overview of NPC Architecture and a Novel Assay for Detecting Interactions between FG Domains

(A) Diagram of the NPC and the FG nups used in this study. *S. cerevisiae* FG nups are shown on the left with vertical tick marks corresponding to individual FG motifs. The numbers above each nup correspond to the aa residues flanking the FG domains used. A cross-section of the NPC is shown with its ring scaffold, its cytoplasmic fibers, a putative meshwork of FG-domain filaments in its center, and the nuclear basket structure.

(B) Models of FG-domain function as architectural elements of the NPC permeability barrier. The virtual-gate model proposes that FG domains are noncohesive, entropic bristles that repel the entry of non-karyophilic proteins into the NPC through Brownian motion. The selective-phase model proposes that FG domains interact with each other via hydrophobic attraction between FG motifs to create a filamentous meshwork that sieves particles by size exclusion.

(C) In vitro assay that detects low-affinity protein interactions. Soluble CFP-FG domain fusions are mixed with bead-immobilized GST-FG nups and the interactions are visualized in a fluorescence microscope under equilibrium binding conditions. A halo of fluorescence around the beads indicates binding between soluble and immobilized nups, whereas dark beads indicate no binding.

a specific subset interacts under physiological conditions to form a cohesive meshwork. Their ability to interact is governed by the type of FG motif and by the aa composition between FG motifs. We also demonstrate that the FG domains of nups are structural components of the NPC permeability barrier in vivo. Our findings support a unified model of NPC architecture featuring two types of gates that restrict diffusion of non-karyophilic proteins across the NPC, one that operates as a selective phase in the NPC center and the other that operates as a virtual gate at the NPC periphery.

RESULTS

The architectural arrangement of FG nups within the NPC has been a subject of much speculation given their central

role in nucleocytoplasmic transport and their presumed role in the NPC permeability barrier (Weis, 2003). Here we addressed the key issue that distinguishes the virtual-gate and selective-phase models of NPC architecture, namely, whether the FG domains of nups bind to each other or not. This question is physiologically relevant because each NPC contains ~175 natively unfolded FG domains that may extend 50 to 200 nm in length as stretched filaments (Denning et al., 2003). Thus, the FG domains of nups are within reach of each other despite being anchored at different sites in the NPC ring scaffold, which is 100 nm wide and 33 nm tall in yeast (Yang et al., 1998).

If the FG domains of nups interact at the NPC to form a meshwork, then their binding affinity must be sufficiently weak to permit the entry and passage of karyopherin-cargo complexes across the NPC. Current protein interaction assays are unsuitable for detection of low-affinity interactions because weakly bound proteins dissociate quickly during the washes that remove unbound proteins. To overcome this limitation, we developed an assay that detects low-affinity interactions in real-time under equilibrium binding conditions. In this assay, GST-nups immobilized at high concentrations on the surface of Sepharose beads are mixed with soluble fluorescent CFP-nups and examined directly under a microscope (Figure 1C). When a CFP-nup binds to an immobilized GST-nup, the interaction is visible as a halo of fluorescence around the dark bead. To avoid nonspecific interactions the assays are performed at neutral pH, with BSA as a blocking agent, EDTA to reduce cation-mediated interactions, salt to disrupt weak ionic interactions, and a low concentration of 1,6-hexanediol to disrupt weak hydrophobic interactions.

Using the low-affinity assay, we examined CFP-nups for their ability to bind immobilized GST-nups (Figures 2 and 3). As controls we used soluble CFP-MBP (Maltose-binding Protein) and immobilized GST (a pair of proteins that do not bind to each other) and Kap95, which binds to all FG nups (Allen et al., 2001). As expected, the bead-immobilized GST did not capture CFP-nup fusions (Figure 2, top row) and soluble CFP-MBP did not bind to immobilized GST-FG nups (Figure 2, left column). By contrast, soluble Kap95-YFP bound to all immobilized FG nups (Figure 2, right column), and all soluble CFP-nups bound to immobilized GST-Kap95 (Figure 3, bottom row).

When the FG-domain interactions were tested (Figure 2; Table S1), the SAFGxPSFG domain of Nup42 and the GLFG domains of Nup116, Nup100, Nup145N, Nup57, and Nup49 bound to each other in all pairwise combinations. The FG domains of Nup100 and Nup116 showed the strongest interactions (Figure 2, central panels), including binding to Nup59, which has four scattered FG motifs. The interactions were detected in buffers with different salt concentrations (100 to 300 mM) and at various temperatures (10°C to 30°C) (data not shown).

In contrast to the GLFG domains of nups, the FxFG domains of Nup60, Nup1, Nup2, and Nsp1 did not bind to GLFG nups, or to SAFGxPSFG nups, or to each other (Figure 2; Table S1). An exception was the homotypic Nup2 interaction and the previously characterized Nup60-Nup2 interaction (Denning et al., 2001). Finally, the SAFGxPSFG domain of peripheral Nup159 showed no binding to other FG domains or to itself (Figure 2; Table S1).

The binding affinities between the cohesive FG domains were estimated to be weak. For instance, the interaction between Nup2 and Nup60 (K_D = 0.4 μM) (Denning et al., 2001) was the strongest detected between nups in the low-affinity assay, but it was mediated by non-FG domains of Nup60. The observed FG-domain interactions were weaker and ranged between K_D = 5 and 70 μM (see below). Although weak, these interactions are physiologically significant because the concentration of FG domains at the NPC is estimated at 1 mM. As expected for such weak affinities, a rapid wash of the beads caused a near-complete loss of inter-FG-domain interactions, whereas high-affinity (K_D ~ nM) karyopherin-FG-domain interactions were unaffected (see examples in Figure S1).

The Cohesive GLFG Domains of Nups Also Bind to a Subset of non-FG Nups

In general, FG nups are anchored at the NPC via folded domains in their termini. In addition, the GLFG domains of nups bind to the non-FG nup Nup85 (K_D = 1.5 μM) (Allen et al., 2002), which is part of the NPC ring-scaffold. The low-affinity assay was used to test if GLFG domains interact weakly with additional non-FG nups. Indeed, the Nup100 and Nup116 FG domains bound to Nic96, Nup84, Nup120, Seh1, Nup170, and Nup85 (Figures 3 and S6; Table S1), though binding to Nup85 was weaker than expected due to a known interference of the GST tag on Nup85 interactions (data not shown). Binding was also detected between (1) Nup84 and the FG domains of Nup42 and Nup57, (2) Nic96 and the FG domain of Nup57, (3) Nup85 and Nup2, and (4) Nup2 and Nup170. Other non-FG nups such as Gle1 and Gle2 and fragments of Nup157, Nup192, Pom34, and Ndc1 did not bind to any of the FG domains (Figure 3; Table S1).

Molecular Basis for the Interaction between FG Domains

The selective-phase model of NPC architecture suggests that FG domains of nups interact via hydrophobic attraction between Phe residues in FG motifs. Although this prediction did not hold true for the FxFG domains, it did for the GLFG domains (Figure 2). GLFG domains contain very few hydrophobic aa, so the GLFG motif itself stands out as the predominant conserved hydrophobic element (Denning et al., 2003; Denning and Rexach, 2007). Thus, the GLFG motifs of two representative GLFG domains were mutated to assess the role of Leu and Phe residues in GLFG-domain interactions (Figure 4A). Site-directed mutagenesis and de novo gene synthesis were used to create all-Phe-to-Ala (F>A) and all-Leu-to-Ala (L>A) mutants of Nup116 and Nup100 GLFG domains (Figure S2). As expected, the bead-immobilized wild-type (WT) Nup116 and Nup100 GLFG domains bound to fluorescent GLFG domains of Nup116, Nup100, and Nup57 and to the SAFGxPSFG

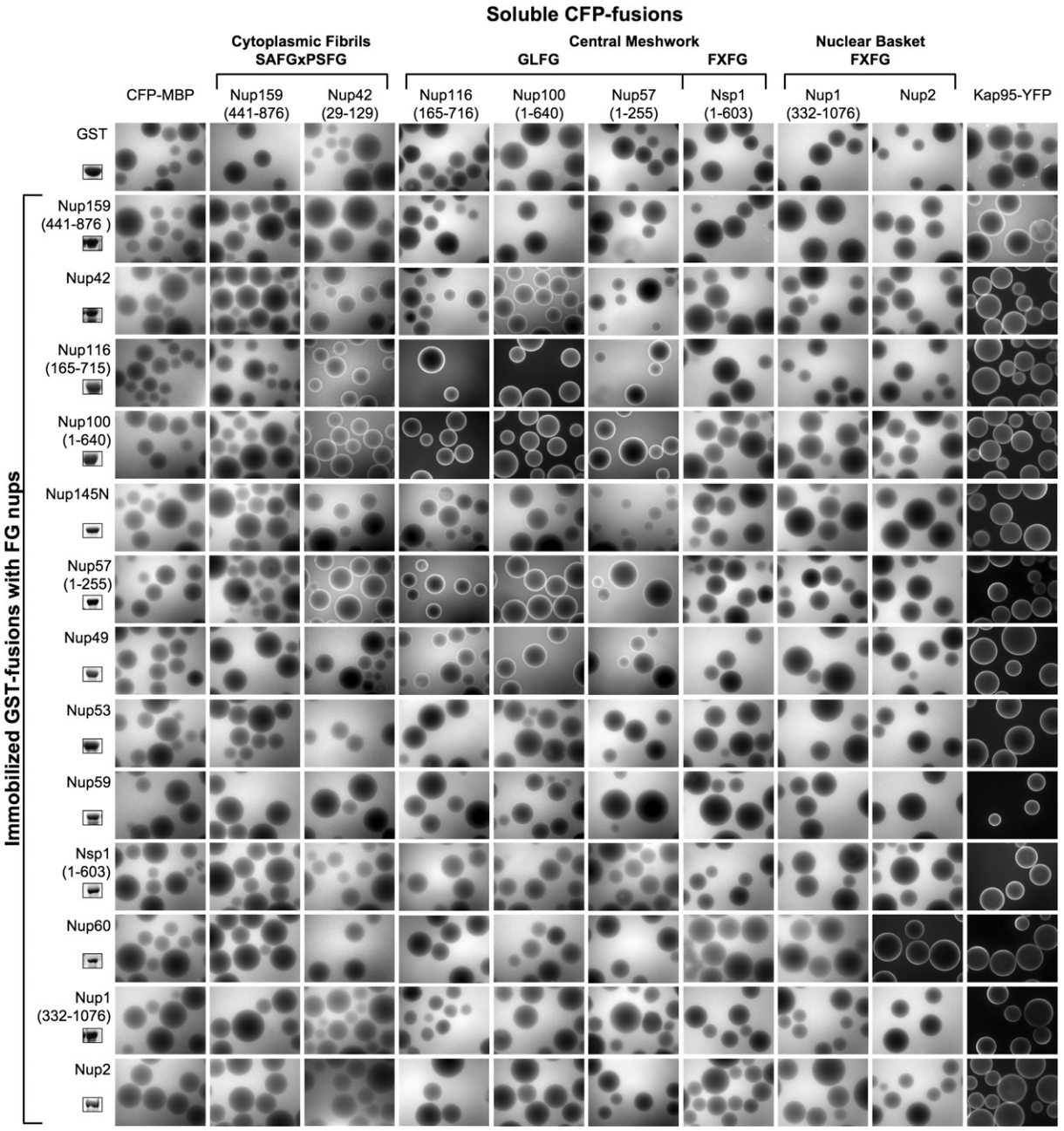

Figure 2. Low-Affinity Interactions between FG Domains

Soluble CFP-FG domain fusions (top row) were mixed with bead-immobilized GST-FG nups (left column). The mixtures were imaged under a fluorescence microscope at 25°C under equilibrium binding conditions. Fluorescent halos indicate positive interactions. Results were categorized as described in Figure S6 and are summarized in Table S1. An aliquot of the immobilized protein was resolved by SDS-PAGE, stained with Coomassie blue, and shown on the left. Sepharose beads are 50–150 μm in diameter.

domain of Nup42 (Figure 4B). By contrast, the immobilized F>A and L>A mutant versions did not, indicating that LF motifs are necessary for GLFG-domain interactions.

The role of Phe residues as "hydrophobic cohesion elements" in GLFG-domain interactions was tested using conservative F>W and F>Y mutations (Figure S2), which changed the aa sequence of the nup but maintained its overall hydrophobicity. These mutants bound to the CFP-GLFG nups just as well as WT (Figure 4B), suggesting that hydrophobicity is a dominant feature in GLFG-domain interactions. When all-Gln-to-Ser mutants were tested, which replaced ~25% of all aa between FG motifs, the binding interactions with CFP-FG domains were unaffected (Figure 4B).

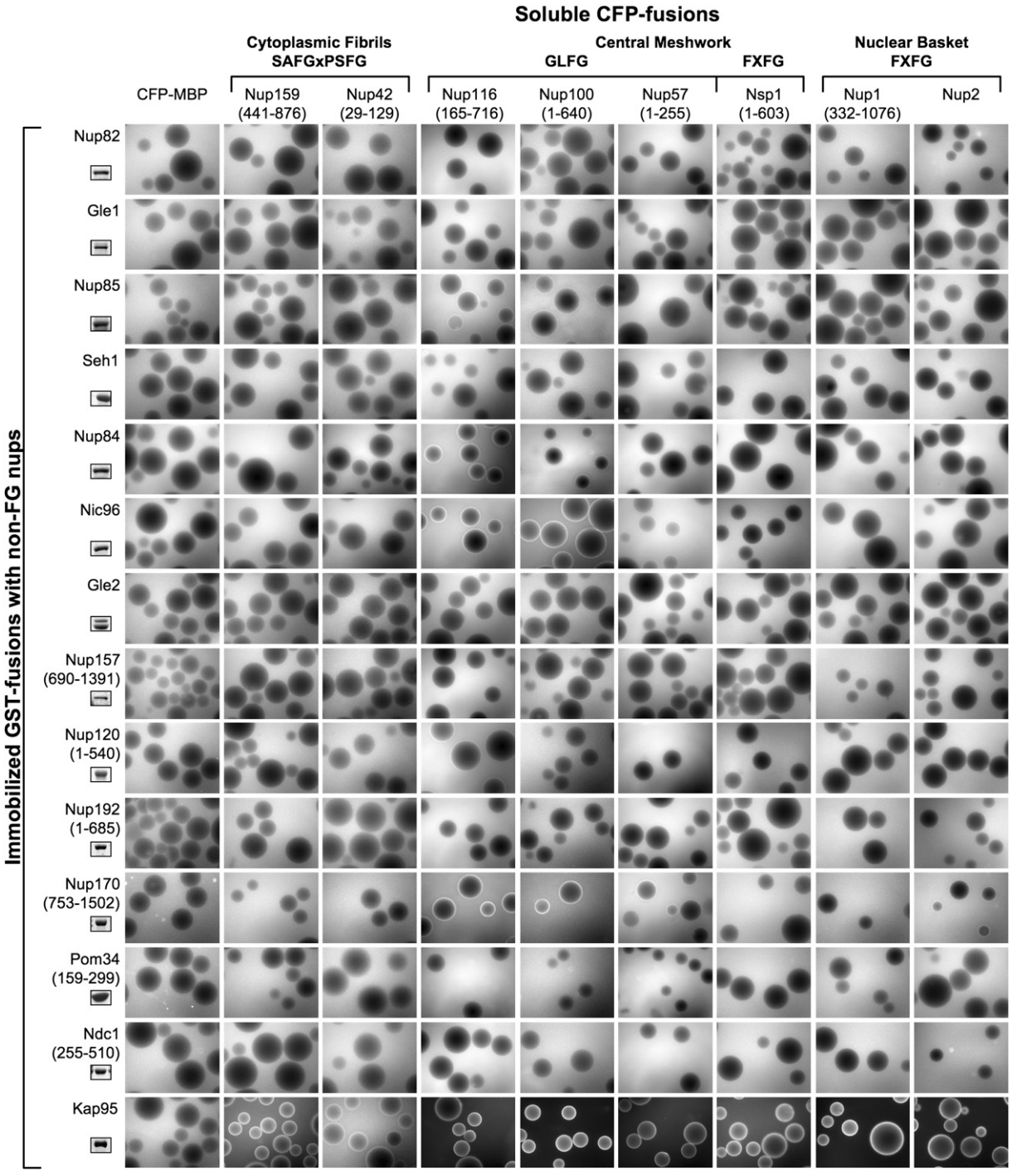

Figure 3. Low-Affinity Interactions between FG Domains and Non-FG Nups

Soluble CFP-FG domain fusions were mixed with bead-immobilized non-FG nups as indicated. Experiments were done and analyzed as in Figure 2.

In Vivo Interaction between FG Domains

Since the GLFG domains of nups formed low-affinity interactions in vitro (Figure 2), we tested whether such interactions could also occur in vivo. Nup FG domains uncoupled from their NPC anchor domains were overexpressed in yeast as YFP-fusions, and their ability to cluster (via homotypic interactions) was monitored visually (Figure 5A). The expression of each fusion was confirmed by western blot analysis, except for YFP-Nup1 (352–1076) and YFP-Nup2 (185–527), which were lethal (data not shown). The cellular

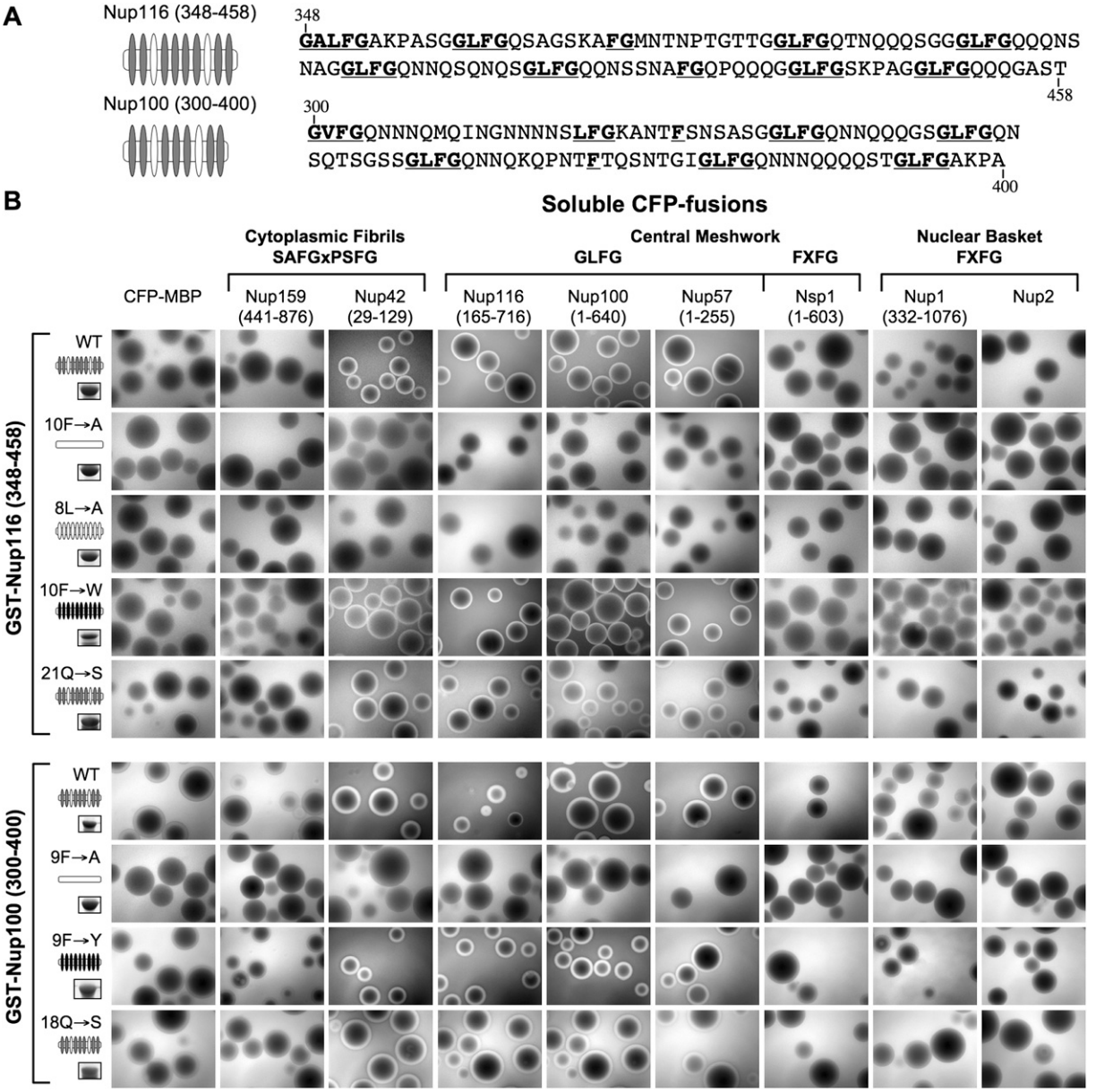

Figure 4. Molecular Basis for the Interaction between FG Domains

(A) Diagram of GLFG domains used for the analysis. Nup116 (aa 348–458) and Nup100 (aa 300–400) are shown with tick marks representing individual FG motifs. Gray tick marks indicate GLFG motifs and white tick marks indicate FG motif variants (xxFG). aa sequences of the GLFG domains used are shown with FG motifs underlined.

(B) Low-affinity interactions between GLFG-domain mutants. Soluble CFP-FG domain fusions were incubated with bead-immobilized GST-Nups or mutant versions thereof, as indicated. The mutant sequences are shown in Figure S2; they were all-Phe-to-Ala substitutions (Nup116 10F>A; Nup100 9F>A), etc., as indicated. Experiments were done as in Figure 2. Black tick marks indicate mutant WG or YG motifs.

distribution of YFP-nups containing the FxFG domain of Nsp1 or Nup60, or the SAFGxPSFG domain of Nup159 or Nup42, was homogenously diffuse, indicating no homotypic interaction. The YFP-SAFGxPSFG domain fusions also accumulated diffusely in the nucleoplasm. By contrast, the YFP-fusions containing GLFG domains of Nup116, Nup100, Nup145N, Nup57, or Nup49 formed cytoplasmic aggregates, indicative of homotypic interactions. When the FG domains of Nup116 and Nup100 were coexpressed as YFP- and CFP-fusions, they formed aggregates that colocalized, indicating heterotypic interactions (Figure 5B). When the CFP-GLFG domains of Nup100 or Nup116 were tethered to membranes through a lipid anchor, the untethered YFP-GLFG domains, but not

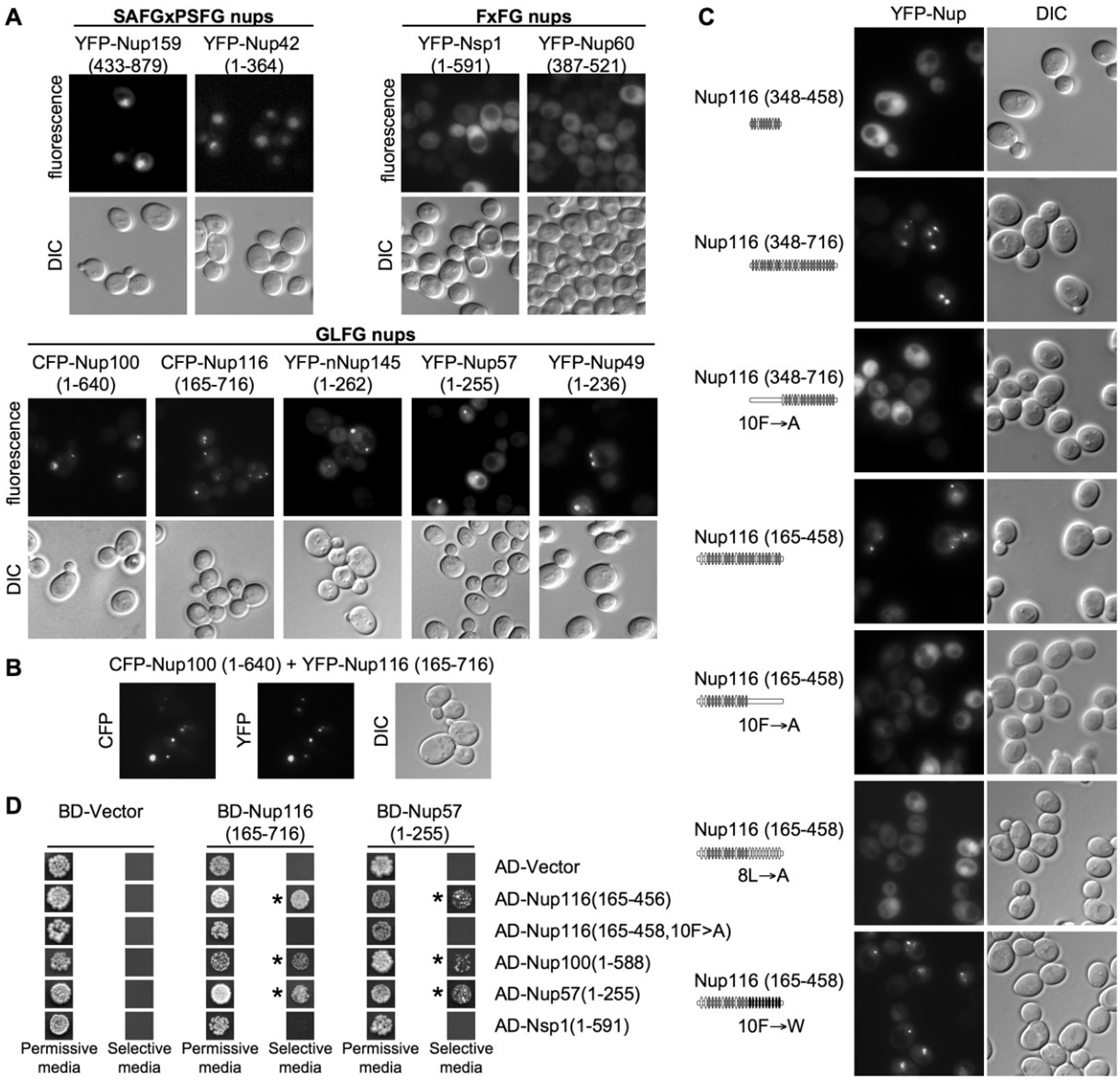

Figure 5. GLFG Domains Interact In Vivo

(A) Homotypic FG-domain interactions. Wild-type yeast expressing CFP- or YFP-FG domain fusions were grown at 30°C to log phase and imaged directly under a fluorescence microscope.

(B) Heterotypic FG-domain interactions. Yeast coexpressing the FG domains of Nup100 and Nup116 as CFP and YFP-fusions, respectively, were imaged as above.

(C) In vivo GLFG-domain interactions require Phe and Leu residues in GLFG motifs. Phe and Leu residues in the aa 348–458 region of Nup116 were replaced as indicated. Wild-type yeast expressing YFP-Nup116 fragments or mutant versions thereof were grown at 30°C to log phase and imaged as above. Nup116 FG-domain diagrams with tick marks representing FG motifs are shown.

(D) GLFG domains form homotypic and heterotypic two-hybrid interactions in vivo. Yeast containing plasmids that express the Gal4-binding domain (BD) and the Gal4 activation domain (AD) were spotted onto permissive media, which selects only for the presence of the two plasmids, or onto selective media, which selects for positive two-hybrid interactions (indicated by asterisks). The expression of the BD- and AD-fusions were verified by western blot analysis (not shown).

the Nsp1 FxFG domain or the Nup116 F>A mutant, were redirected to form aggregates at membranes (Figure S4), demonstrating that the cytoplasmic aggregates represent FG-domain oligomers rather than cellular scavenging sites. We conclude that nup GLFG domains form homotypic and heterotypic interactions in vivo.

To test if FG motifs are necessary for GLFG-domain interactions in vivo, WT and F>A mutant versions of Nup116

aa 348–458 were overexpressed in yeast as YFP-fusions and scored for clustering as above (Figure 4A). Unexpectedly, the WT version, which has ten FG motifs and is self-cohesive in vitro (Figure 4B), was diffusely distributed in vivo (Figures 5C and S3), indicating no homotypic aggregation. Since a difference in sensitivity between the in vivo and in vitro binding assays might explain this apparent discrepancy, we increased the size of the FG domains to contain more FG repeats. The larger Nup116 aa 165–458 and aa 348–716 FG domains, which contain 24 and 27 FG motifs, respectively, and mutant versions thereof lacking 10 Phe (F>A or F>W) or 8 Leu (L>A) residues in the aa 348–458 region (Figure 5C) were overexpressed in yeast as YFP-fusions. The WT FG domains clustered in the cytoplasm, indicating homotypic cohesion, but the F>A and L>A mutants did not, indicating noncohesion. The F>W mutants also aggregated, consistent with the in vitro results (Figure 4).

A second test of in vivo interactions between FG domains was conducted using the yeast two-hybrid system, which detects protein interactions as weak as K_D = 70 μM (Yang et al., 1995). Various FG domains fused to the DNA-binding domain (BD) or the transcription activation domain (AD) of Gal4 were transformed as pairs into a two-hybrid reporter yeast strain. The strains were then analyzed for growth on selective media, where growth depends on positive two-hybrid interactions. As expected, neither the Gal4 DNA BD nor the AD alone produced two hybrid signals. In contrast, the Nup116 GLFG domain (BD-Nup116) interacted with itself and with the GLFG domains of Nup100 and Nup57 but not with the Nsp1 FxFG domain (Figure 5D). Likewise, the Nup57 GLFG domain (BD-Nup57) interacted with itself and with the GLFG domains of Nup100 and Nup116 but not with the Nsp1 FxFG domain. Lastly, none of the FG domains interacted with the Nup116 aa 165–458 F>A mutant, demonstrating that the interactions detected are specific and sensitive to the number of FG motifs present. Additional tests of FG-domain interactions were not possible due to self-activation or toxicity issues, which limit two-hybrid analyses. Importantly, the two-hybrid results matched well with the results obtained with the low-affinity protein interaction assay (Figures 2 and 4) and therefore validated the FG-domain interactions detected in vitro. It also established a lower limit for the weak affinity between FG domains at K_D ~70 μM (the detection limit of the two-hybrid assay).

GLFG-Domain Interactions Are Disrupted by Hexanediol

Hexanediol weakens the NPC permeability barrier in cells (Ribbeck and Gorlich, 2002; Shulga and Goldfarb, 2003), presumably by interfering with FG-domain interactions. Indeed, as predicted, 1,6-hexanediol blocked interactions between GLFG domains in vivo (Figure 6B). Also, the FG-domain interactions detected in vitro, including the interactions with non-FG nups, were disrupted by 1,6-hexanediol (Figure 6A, data not shown). For example, the robust interaction between soluble CFP-Nup100 FG domain and immobilized GST-Nup116 FG domain was completely abolished (Figure 6A). Similarly, *trans*-1,2-cyclohexanediol also disrupted the interactions, whereas the less hydrophobic 1,2,3-hexanetriol did not (Figure S5B). In vivo, the cytoplasmic aggregates of GLFG domains dispersed quickly (<1 min) after addition of 1,6-hexanediol to the culture medium (Figure 6B, data not shown). The effect was fully reversible, as removal of hexanediol allowed the rapid re-aggregation of FG domains. The solubility of FG-domain aggregates in hexanediol distinguishes them from other types of aggregates, such as prion amyloids (e.g., of Sup35), which did not dissolve in 1,6-hexanediol (Figure 6B) or even SDS (Serio et al., 2000). Ethanol and *trans*-1,2-cyclohexanediol, but not 1,2,3-hexanetriol, also dissolved the FG-domain aggregates in vivo (Figure S5). In particular, the effect of ethanol on aggregate dispersal was fast and fully reversible for at least two cycles within 10 min (Figure S5). Hence, the disaggregating effect of the alcohols was not due to a cellular stress response. Consistently, a 15 min heat shock at 37°C or 42°C had no effect on the aggregates (data not shown).

The FG Domains of Nups Are Functional Elements of the NPC Permeability Barrier

If the filamentous FG domains of nups are necessary to maintain the NPC permeability barrier in vivo, then their removal should relax the barrier. In yeast, proteins smaller than 40 kDa easily cross the NPC by passive diffusion, whereas larger proteins cannot. This can be observed in cells using fluorescent proteins of different sizes (Shulga and Goldfarb, 2003; Shulga et al., 2000). This visual assay is ideal for the detection of gross changes in the NPC permeability barrier but may not detect subtle changes. Hence, we developed a more sensitive NPC permeability assay based on the yeast one-hybrid system (Figure 7A). The yeast Gal4 transcription AD was fused to the bacterial DNA-binding protein LexA, which was modified to remove a cryptic NLS (mLexA) (Rhee et al., 2000). Since LexA is a dimer (Mohana-Borges et al., 2000), the resulting mLexA-Gal4AD chimera is 70 kDa and is excluded from entering the nucleus. However, when the NPC permeability barrier is compromised, the chimera gains access to the nucleoplasm and drives *lacZ* expression. The resulting β-galactosidase (β-gal) activity is easily quantified in cell extracts and provides a measure of NPC permeability defects. Since the cellular expression of mLexA-Gal4AD and β-gal are affected equally by strain-specific differences in gene expression, mRNA processing, mRNA export, and/or protein translation, those differences could be corrected by normalizing the β-gal activity to the amount of LexA activator in each strain.

As expected, there was some "leakage" of mLexA-Gal4AD into the nucleus of WT yeast, enough to give a quantifiable β-gal signal (Figure 7B). When a cNLS was fused to mLexA-Gal4AD to increase its nucleoplasmic concentration, the β-gal activity increased nearly 10-fold

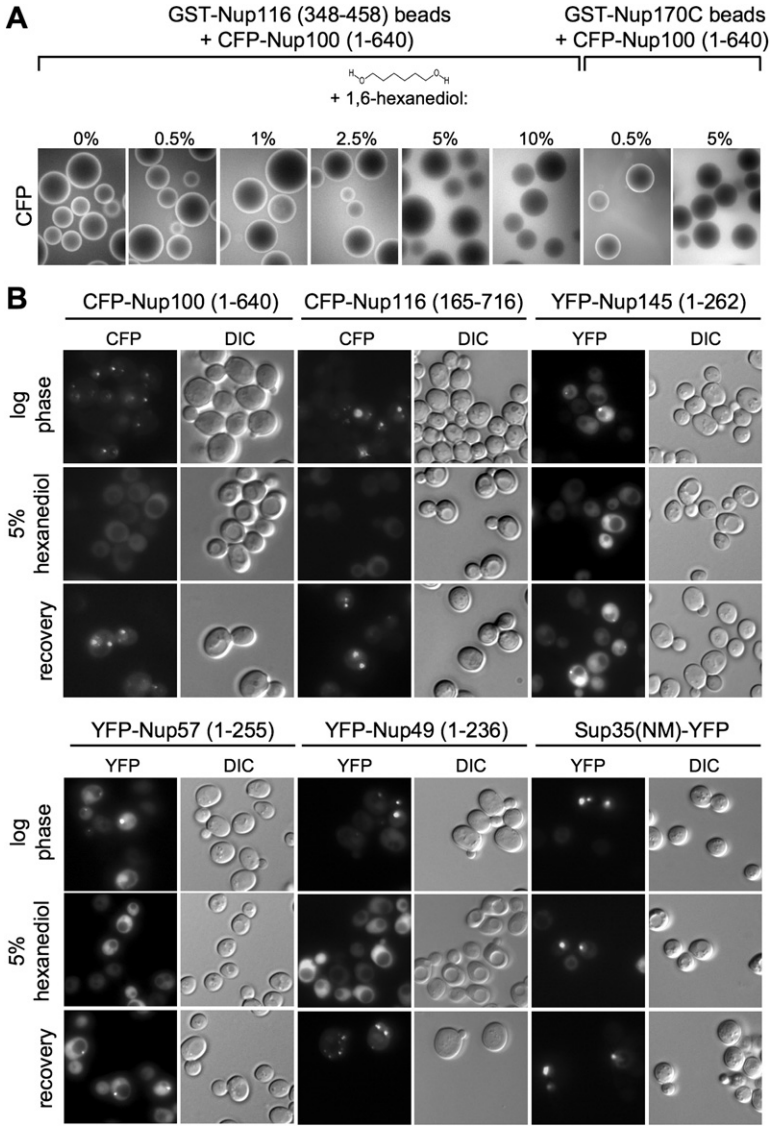

Figure 6. The In Vitro and In Vivo Associations between GLFG Domains of Nups Are Disrupted by Aliphatic Alcohols

(A) Effect of 1,6-hexanediol on FG-domain interactions in vitro. Soluble CFP-Nup100 (aa 1–640) was incubated with immobilized GST-Nup116 (aa 348–458) or GST-Nup170 (aa 753–1502) in the presence of 1,6-hexanediol.

(B) Effect of 1,6-hexanediol on FG-domain interactions in vivo. CFP- and YFP-tagged FG domains or Sup35NM-YFP were expressed individually in yeast at 30°C. During the log phase of growth, 1,6-hexanediol was added to the growth media and the yeast were imaged 10 min later. The same results were obtained when the yeast were imaged in < 1 min (not shown). Where indicated yeast were collected, resuspended in fresh media, incubated at 30°C for 10 min without hexanediol, and visualized as before (recovery).

(data not shown). This demonstrates that an increase in nuclear concentration of mLexA-Gal4AD can be quantified above background. To validate the new assay, we tested *nup170Δ* yeast and yeast treated with 1,6-hexanediol, two conditions that relax the NPC permeability barrier in vivo (Shulga and Goldfarb, 2003). As expected, the *nup170Δ* yeast contained more β-gal activity than control isogenic WT yeast (Figure 7B), indicating that *nup170Δ* cells have a partially disrupted NPC permeability barrier. Also as expected, the exposure of WT and *nup170Δ* yeast to 5% 1,6 hexanediol caused an increase in β-gal activity in both strains (Figure 7B). These results validated the new assay and confirmed that the NPC permeability barrier is disrupted by 1,6-hexanediol and that the effect is exacerbated in *nup170Δ* yeast (Shulga and Goldfarb, 2003).

The integrity of the NPC permeability barrier was tested in *ΔFG* yeast lacking the GLFG domain of Nup116 or Nup100, the SAFGxPSFG domain of Nup42, or the FxFG domain of Nsp1, Nup60, Nup1, or Nup2. The *nup116ΔFG*, *nup100ΔFG, nup60ΔFG*, and *nup1ΔFG* yeast showed NPC permeability barrier defects, judging from their elevated content of β-gal activity. After exposure to hexanediol, each of the *ΔFG* yeast produced more β-gal activity than WT. Thus, hexanediol exacerbated an underlying defect in their NPC permeability barrier. Together, the results suggest that the FG domains of peripherally and centrally anchored nups establish or maintain the NPC permeability barrier.

Since deletion of either type of FG domain (cohesive and noncohesive) compromised the NPC permeability barrier, we tested whether *cohesion* between FG domains in situ at NPCs, rather than just their *presence,* is important for the permeability barrier. The cohesive FG domain of Nup100 was substituted by the noncohesive, equally

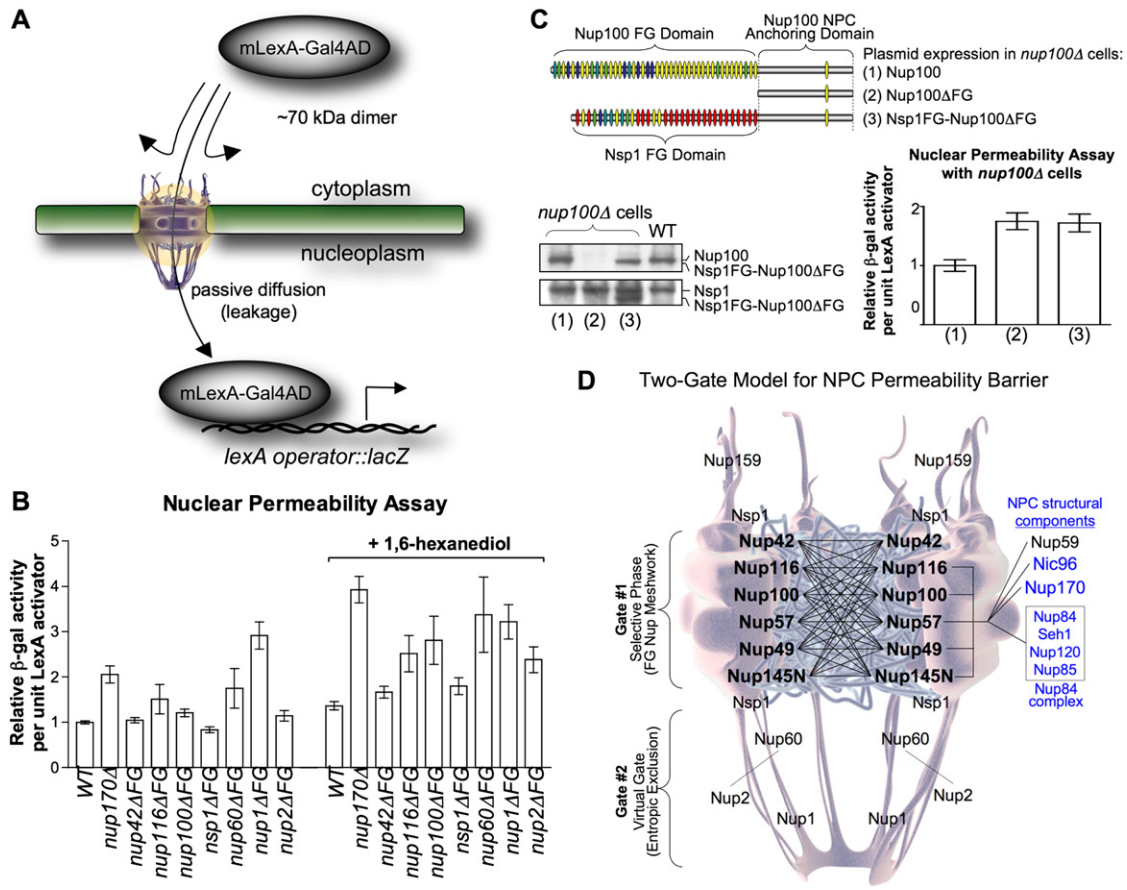

Figure 7. Yeast Lacking Nup FG Domains Display NPC Permeability Barrier Defects

(A) An assay that monitors the integrity of the NPC permeability barrier in vivo. A non-karyophilic protein of 70 kDa (mLexA-Gal4AD) can enter the nucleus only by passive diffusion through NPCs. In the nucleoplasm, it activates transcription of the *lacZ* gene from a LexA promoter. The resulting β-gal activity is quantified in cell extracts and reflects the extent of mLexA-Gal4AD "leakage" into the nucleoplasm.

(B) The effect of FG-domain deletions on the NPC permeability barrier. WT and mutant yeast lacking the indicated FG domains were transformed with one-hybrid plasmids and grown at 30°C to log phase. The yeast were then exposed (or not) to 1,6-hexanediol for 30 min at 30°C and were harvested after 1.5 hr of growth at 30°C in alcohol-free media. The β-gal activity in cell extracts was quantified, and the values were normalized against the expression level of LexA activator for each strain. Mean data ± SEM are plotted relative to WT = 1.

(C) The cohesion of FG-domain filaments at the NPC is necessary for proper NPC permeability barrier function. The integrity of the NPC permeability barrier was assayed in *nup100Δ* yeast containing plasmids that express (1) full-length Nup100, (2) Nup100 lacking its FG domain (Nup100ΔFG), or (3) Nup100 with its FG domain replaced by the Nsp1 FG domain (Nsp1FG-Nup100ΔFG). Schematics of these proteins are shown. The expression of Nup100 and Nsp1 in the individual strains was confirmed by western blot analysis using anti-Nsp1 and anti-Nup100 antibodies. Expression of the Nup100 anchor domain (Nup100ΔFG) was also confirmed by western blot analysis (not shown). Experiments were done as in (B). Mean data ± SEM are plotted relative to WT = 1.

(D) Two-gate model for NPC architecture and web diagram of a low-affinity "interactome" detected in this study. Nups are positioned in the NPC according to their anchor sites. The FG domains of nups (in black bold font) form a web of low-affinity interactions (indicated by lines) with each other and with a discrete subset of non-FG nups (in light blue font). In our two-gate model, the FG domains of nups that are anchored at the NPC center form a cohesive meshwork of filaments, as hypothesized by the selective-phase model, whereas the FG domains of nups anchored at the nuclear basket structure do not interact and behave as repulsive filaments, as hypothesized by the virtual-gate model.

long Nsp1 FG domain to create the chimera Nsp1FG-Nup100ΔFG (Figure 7C). When Nup100, Nup100ΔFG, or Nsp1FG-Nup100ΔFG were expressed from a plasmid in *nup100Δ* yeast, which lack endogenous Nup100, the cells expressing Nup100ΔFG and Nsp1FG-Nup100ΔFG had a compromised NPC permeability barrier relative to cells expressing full-length Nup100 (Figure 7C). We conclude that *cohesion* between FG domains in situ at NPCs is an important element of the permeability barrier.

DISCUSSION

We investigated the role of FG nups as functional elements of the NPC permeability barrier. Our analysis was

focused on their large FG domains, which exist in their native state as highly flexible filaments devoid of ordered secondary structures (Denning et al., 2003). Using a novel in vitro assay that detects specific, low-affinity protein interactions (Figure 1C), we showed that the FG domains of five out of six FG nups anchored at the NPC center (Nup100, Nup116, Nup57, Nup49, and Nup145N), plus the FG domain of Nup42, which is anchored at the cytoplasmic fibrils, bind to each other in vivo and in vitro via hydrophobic attractions (Figures 2–5; Table S1). We suggest that these FG domains of nups form a cohesive meshwork of filaments at the NPC center (Figure 7D). This finding provides a key piece of evidence in support of the selective-phase model of NPC architecture (Figure 1B).

Using a novel assay that monitors the NPC permeability barrier in *live* yeast, we demonstrated that the FG domains of nups anchored at central and peripheral locations of the NPC cooperate to establish a protein diffusion barrier (Figure 7). The results support the hypothesis that ~175 FG nups in each NPC function collectively as a filamentous sieve to sort particles by size exclusion (Denning et al., 2003). As deletion of any individual FG domain from the NPC reduces the total number of FG nup filaments by 8, 16, or 24, etc., depending on its copy number within the NPC (Rout et al., 2000), we expected that each individual FG-domain deletion would have only a minor defect in the NPC permeability barrier, as observed (Figure 7B). In some cases, the NPC permeability defects in the mutants were detected only after the cells were exposed to hexanediol (Figure 7B). This suggests that, in addition to the number of FG-domain filaments, their ability to form a *cohesive* meshwork at the NPC is important for maintaining the NPC permeability barrier. To best address the issue of whether *cohesion* between FG domains is critical for the permeability barrier, we demonstrated that replacing a cohesive FG domain (from Nup100) with a noncohesive FG domain (from Nsp1) caused a permeability barrier defect (Figure 7C).

The interaction between FG domains was dispersed by 1,6-hexanediol in vivo and in vitro (Figure 6). This provided a molecular explanation for the observed NPC permeability barrier defects in yeast exposed to 1,6-hexanediol (Shulga and Goldfarb, 2003). When we tested various forms of hexanediol for their ability to disperse FG-domain interactions, we noted that 1,6-hexanediol and *trans*-1,2-cyclohexanediol were equally effective (Figures 6 and S5). In contrast, 1,2-hexanediol caused visible damage to yeast, aggregation of CFP- and YFP-fusions in vivo and in vitro, and nonspecific interactions between nups and proteins such as CFP and MBP (not shown). Notably, 1,2-hexanediol was used for the NPC permeability barrier experiments in perforated mammalian cells (Ribbeck and Gorlich, 2001) and for the biophysical experiments on the purified FxFG domain of human Nup153 (Lim et al., 2006). Based on our observation, it seems likely that the effects of 1,2-hexanediol in those cases were caused by nonspecific adhesions of FG domains with neighboring proteins or with themselves, rather than by specific effects on FG motif interactions.

Another key piece of evidence in support of the selective-phase model of NPC architecture was our demonstration that the interactions between GLFG domains of nups require Phe residues in GLFG motifs (Figures 4 and 5). Beyond that, the Leu residues in GLFG motifs were also important for the FG-domain interactions. Interestingly, F>W and F>Y substitutions in GLFG motifs did not abolish the interactions, indicating that the hydrophobicity of Phe residues in FG repeats is more important than the specific side-chain structure. Finally, substitution of nearly 25% of aa in between GLFG repeats (e.g., in the Q>S mutants) did not affect the interactions (Figure 4), suggesting that aa in between FG motifs are not directly involved in FG-domain interactions.

Perhaps not surprisingly, the GLFG domains of nups anchored at the NPC center interacted with a subset of non-FG nups that form the ring scaffold surrounding the central conduit of the NPC (Figure 3; Table S1). We propose that these interactions maintain a seal between the meshwork of FG-domain filaments at the NPC center and the inner walls of the NPC ring scaffold. Indeed, when the seal was disrupted by mutation (e.g., as in *nup170Δ* yeast) or by hexanediol, the permeability barrier was functionally compromised (Figure 7) (Shulga and Goldfarb, 2003).

Contrary to a central prediction made by the selective-phase model (i.e., that all FG domains of nups interact by virtue of their FG motifs), we demonstrated here in vivo and in vitro that some FG domains of nups are not cohesive, including the FxFG domains of Nsp1, Nup1, Nup2, and Nup60 and the SAFGxPSFG domain of Nup159 (Figures 2–5 and S4). This finding supports the notion that some FG domains of nups function exclusively as repulsive bristles due to Brownian motion, consistent with the virtual-gate model (Rout et al., 2000). Indeed, it was recently shown that the isolated FxFG domain of the human Nup153 (the yeast Nup1 ortholog) is noncohesive and sterically repulsive (Lim et al., 2006).

The recent demonstration by Frey et al. that the FG domain of Nsp1 can form homotypic interactions in the form of a hydrogel would seem to support the selective-phase model (Frey et al., 2006). However, the nonphysiological conditions that were necessary to generate the hydrogel make it unlikely that a similar Nsp1 structure could form in yeast. In fact, we demonstrated here using three different in vivo tests and one in vitro test that the Nsp1 FG domain does not form interactions with other FG domains or with itself (Figures 2, 5A, 5D, and 7C) even at high concentration (~500 μM) (data not shown).

Our finding that FxFG domains of nuclear basket nups (Nup1, Nup2, and Nup60) are functional elements of the NPC permeability barrier (Figure 7B) supports the virtual-gate model because these FG domains behave as noncohesive filaments (Figures 2 and 5A). However, what was not envisioned in that model was the location of the virtual gate at the "exit site" of the NPC, rather than at the "entry site." Our finding implies that non-karyophilic proteins that somehow gain access to the NPC center can still be denied nuclear entry by the FG nups of the

distal basket structure. Our results contrast previous work, which reported no visible defects in the NPC permeability barrier in yeast missing five FG domains of nups in peripheral NPC structures (*nup159ΔFG nup42ΔFG nup60ΔFG nup1ΔFG nup2ΔFG*) (Strawn et al., 2004). We suggest that our assay detected the function of these nups because it monitors the integrity of the NPC permeability barrier with much greater sensitivity due to its physiological and constitutive test conditions (i.e., over the lifetime of yeast), rather than during a 10 min time-window after chilling or depleting ATP from cells, as in the visual NPC permeability assay used by Strawn et al. Perhaps these treatments, or the different experimental timescales, or differences in the genetic makeup of the yeast strains used could explain the difference. Regardless, the pioneer visual assay (Shulga et al., 2000) and our new genetic assay for NPC permeability (Figure 7) both detected defects in *nup170Δ* yeast and in yeast exposed to 1,6-hexanediol.

Taken together, our data support a two-gate model of NPC architecture (Figure 7D). One gate, formed by the cohesive FG domains of nups anchored at the NPC center, may operate as a size-selective meshwork of filaments held together by hydrophobic attractions between FG motifs (a selective phase). The interactions between cohesive FG domains and structural non-FG nups, such as Nup170, may seal the meshwork against the NPC ring scaffold through multipoint interactions. A second gate, formed by noncohesive FG domains of nups anchored at the NPC periphery, may operate as a virtual gate through the dynamic behavior of noncohesive FG-domain filaments and their Brownian motion. In principle, even the cohesive FG domains of nups could function "part-time" as repulsive bristles as they interconvert between structures in the periphery of the central meshwork. The genetic interaction between the ring scaffold Nup170 and the nuclear basket FxFG nups Nup1 and Nup2 (Kenna et al., 1996), and the biochemical interaction between Nup2 and Nup170 (Figure 3), suggest that the two types of gates may communicate through Nup170. Consistent with our two-gate model, a principal diffusion gate in vertebrate NPCs was mapped to the central region of the NPC using morphological examination of cells that were injected with gold particles of different sizes (Feldherr and Akin, 1997). In the same report, a second gate for large particles was mapped to the nuclear basket structure. Thus, NPCs may contain two types of gates that simultaneously control the diffusion of proteins into and out of the nucleus.

Finally, we searched for a biochemical property in the FG domains that could explain why some FG domains are cohesive whereas others are not. Our report thus far points to the LF motif in GLFG repeats as the cohesive element and predicts that any FG domain with GLFG motifs would be cohesive. However, the FG domain of Nup42 contains no GLFG motifs, yet it is cohesive, and the human FG nups contain almost no GLFG motifs yet form a permeability barrier. To address the possibility that the overall hydrophobicity of each FG domain dictates its cohesive properties, we examined the aa composition of every FG domain in yeast and other organisms (Table S2). Surprisingly, the overall hydrophobicity of a given FG domain is a poor predictor of its interactivity with other FG domains. For example, the noncohesive FxFG domains of Nsp1, Nup1, Nup2, and Nup60 are *more* hydrophobic than the cohesive GLFG domains of Nup116, Nup100, Nup57, Nup49, and Nup145N (Table S2). Thus, a different biochemical property in FG domains must govern their interactions. Indeed, analysis of the cohesive FG domains revealed that they have very few (<3.7%) charged residues in between FG repeats and instead are rich in polar residues. This property is clearly distinct from the noncohesive FG domains, which contain an abundance (>17.7%) of charged residues in between FG motifs. We therefore propose that short hydrophobic patches (provided by LF motifs in the case of GLFG repeats) and a low content of charged residues in between these patches are needed to form cohesive FG domains.

Using the above guidelines as predictors of FG-domain cohesiveness, we ranked all of the FG domains of nups from widely different organisms according to their content of charged residues between FG motifs (Table S2). At the top of each list are the FG nups with the lowest percentage, which are predicted to be cohesive according to our guidelines, and at the bottom of each list are the nups with the highest percentage of charged residues in between FG motifs, which are predicted to be noncohesive according to our guidelines. The predictions of the analysis for *S. cerevisiae* FG nups match perfectly with our experimental results (Table S2). Among the human FG nups, the five nups with the lowest percentage of charged residues in their FG domains (hNup54, hNup62, hNup45, hNup214, and hNup58) are predicted to be cohesive. Interestingly, four of them are anchored at the NPC center (Cronshaw et al., 2002) similar to the cohesive FG nups in yeast. Hence, we suggest that the FG domains of these human nups interact to form a cohesive meshwork of filaments at the NPC center. The other seven human FG nups, including Nup153, contain a higher content of charged residues in between FG motifs and at least five of them are anchored at peripheral structures of the NPC, similar to noncohesive FG nups in yeast. Hence, their FG domains may behave as noncohesive entropic bristles, as observed for human Nup153 (Lim et al., 2006).

EXPERIMENTAL PROCEDURES

Recombinant Proteins

Recombinant nups were expressed as GST-fusions in *E. coli* vector pGEX-2TK (GE Healthcare) and purified as described (Denning et al., 2001). Kap95-YFP and CFP-fusions were purified initially as GST-fusions and GST was removed by thrombin cleavage as described ("GST Handbook," GE Healthcare). The Nup100 and Nup57 CFP-fusions contained a C-terminal 6xHIS tag, which was used to purify these nups further using Nickel beads (this ensures purification of full-length CFP-nup protein without degradation products). All CFP-fusions were ultimately purified by gel filtration in a FPLC Superdex-200

column and concentrated to 0.4–1 mg/ml in binding buffer (20 mM HEPES [pH 6.8], 150 mM KOAc, 2 mM $Mg(OAc)_2$, 1 mM DTT, 0.1% Tween-20) using a Centricon-10 (Millipore).

Low-Affinity Protein Interaction Assay

Purified GST-fusions were loaded onto glutathione-Sepharose beads (GE Healthcare) at a concentration of 5–10 mg per ml of packed beads. After washing, beads were resuspended as a 50% slurry in binding buffer and a 0.75 μl portion of the slurry was mixed with 0.5 μl of EHBN 4× stock buffer (40 mM *E*DTA, 2% 1,6-*h*exanediol, 40 mg/ml *B*SA, 500 mM *N*aCl) and with 0.75 μl of purified soluble CFP-nup to obtain a 2 μl sample to image on a microscope slide. Beads were viewed under a Nikon fluorescence microscope with a 20× air objective using CFP and YFP filters.

In Vivo Expression of Nup FG Domains

The FG domains of Nup159 (aa 441–876), Nup42 (1–364), Nup116 (165–716, 348–458, 165–458, or 348–716), Nup100 (1–640), Nup145N (1–262), Nup57 (1–255), Nup49 (1–236), Nsp1 (1–591), Nup60 (387–521), Nup1 (352–1076), and Nup2 (185–527) were cloned as CFP- or YFP-fusions into pVT102-U or pVT102-LEU2, respectively, which allow constitutive expression from an *ADH1*-promoter in yeast (Vernet et al., 1987). pVT102-LEU2 was made by replacing *URA3* in pVT102-U with *LEU2*. Plasmids were transformed into the WT haploid yeast (BY4741, Research Genetics) that had been previously cured of prions by growth on media containing 5 mM GuHCl (Eaglestone et al., 2000). Transformants were grown to log phase and photographed through a 100× oil objective using CFP or YFP filters in a Nikon microscope. To generate membrane-tethered CFP-fusions, the N-terminal 9 aa of yeast Gpa1 (MGCTVSTQT) were fused to the N terminus of CFP, CFP-Nup100 (1–640), and CFP-Nup116 (165–716). This Gpa1 sequence targets proteins to membranes via N-myristoylation (Gillen et al., 1998).

Generation of Nup116 and Nup100 FG-Domain Mutants

Fragments of the Nup116 FG domain (348–458) and the Nup100 FG domain (300–400) were used as representative GLFG domains. To create the Nup116 10F>A mutant, Phe residues in FG motifs were substituted for Ala using site-directed mutagenesis. Additional mutants (shown in Figure S2) were synthesized de novo (GeneScript). For the in vitro analyses, the Nup116 and Nup100 FG-domain mutants were purified as GST-fusions. For in vivo analyses, the Nup116 aa 348–458 encoding region in pVT102-LEU2::YFP-Nup116 (165–716, 348–458, 165–458, or 348–716) was replaced by mutant Nup116 sequences using ligase-free cloning.

Yeast Two-Hybrid Assay

FG domains (indicated in Figure 5D) were amplified by PCR and fused in-frame to the Gal4 DNA BD in pGBKT7 or to the Gal4 transcriptional AD in pGADT7 (Clontech). BD- and AD-fusions were cotransformed into AH109 yeast (Clontech) and the yeast were grown overnight on plasmid-selective media (SCD −leu −trp). Next day equivalent number of cells were spotted onto permissive media (SCD −leu −trp) and onto selective media, which selects for positive two-hybrid interactions (SCD −leu −trp −his −ade media in the case of BD-Nup116 transformants or SCD −leu −trp +1 mM 3AT media in the case of BD-Nup57 transformants). Plates were scanned after 5 days of growth.

In Vivo NPC Permeability Barrier Assay

DNA containing the mLexA-Gal4AD ORF flanked by *ADH1* promoter and terminator sequences was transferred by ligase-free cloning to pRS423 (HIS3, 2μ plasmid) to generate pNPA (*n*uclear *p*ermeability *a*ssay). A *lexA* operator sequence in front of *lacZ* gene in plasmid pSH18-34 (S. Hanes, personal communication) contains the target site for the one-hybrid activator. Yeast transformed with pNPA and pSH18-34 were grown at 30°C overnight in selective media, diluted next day to a cell density of 0.15 (OD600 units) in ~1 ml of YPD, and grown further in triplicate to a density of 0.5. The alcohol 1,6-hexanediol was added (5%) or not, as indicated. The yeast were grown for another 20 min at 30°C, harvested, resuspended in fresh YPD media without hexanediol, and incubated for an additional 1.5 hr at 30°C. After recording the density of each culture, 100 μl aliquots were vacuum-filtered in a Millipore Multiscreen-HTS 96-well plate to collect cells. Yeast were washed with 200 μl of Z-buffer (60 mM Na_2HPO_4, 40 mM NaH_2PO_4, 10 mM KCl, 1 mM $MgSO_4$, pH 7.0) and resuspended with Z-buffer plus 100 mM β-mercaptoethanol, 0.02% CTAB and 0.01% sodium deoxycholate. After 5 min at 25°C, 20 μl of 4 mg/ml ONPG dissolved in Z-buffer was added to the cell extracts and the β-gal reaction was allowed to proceed at 30°C until reactions turned mild yellow. Reactions were stopped by adding 50 μl of 1 M Na_2CO_3, and the reaction products were transferred to 96-well plates by filtration. The absorbance of each well was measured at 420 nm in a SPECTRAmax plate reader (Molecular Dynamics).

To quantify the amount of mLexA-Gal4AD activator in cells, proteins in whole-cell extracts were resolved by SDS-PAGE, transferred to PVDF membrane, and processed for western blotting using an anti-LexA antibody (Invitrogen). Anti-Nap1 antibodies (gift from Doug Kellogg) were used in parallel to detect Nap1, which served as a protein loading control. After incubation with fluorescent IgG secondary antibodies (Jackson Immunological), the blots were imaged in a Typhoon scanner (GE Healthcare). The amount of LexA and Nap1 was quantified using ImageQuant (GE Healthcare). The amount of LexA in each sample was normalized against the amount of Nap1 in the same sample, and the measured β-gal activity was expressed as relative A420 absorbance units per unit of LexA.

Generation of Nup ΔFG Domain Mutant Yeast

Chromosomal deletions of nup FG domains were done in WT diploid yeast (BY4743) using the Cre-Lox system as described (Strawn et al., 2004). All strains used here though were made in the *S288C* background, which was used in the *Saccharomyces* Sequencing Project and in the Systematic *Saccharomyces* Genome Deletion Project. The aa deleted were Nup42 (2–370), Nup116 (167–715), Nup100 (2–588), Nsp1 (10–603), Nup60 (389–515), Nup1 (332–1040), and Nup2 (186–561). The resulting ΔFG strains were converted into one-hybrid reporter strains by transformation with pSH18-34 and pNPA. To replace the FG domain of Nup100, the *NUP100* gene was amplified together with 756 bp of upstream and 322 bp of downstream sequence and cloned into pRS425. This plasmid produced WT levels of Nup100p expression in *nup100Δ* cells. When indicated, the Nup100 FG domain (aa 2–588) was deleted or replaced with the Nsp1 FG domain (aa 10–603) by PCR.

aa Composition of the Nup FG Domains

FG-domain sequences from *S. cerevisiae*, *H. sapiens, S. pombe*, *C. elegans*, and *D. melanogaster* were subjected to aa composition analysis. Nup sequences were acquired from the *Saccharomyces* Genome Database (yeastgenome.org) (Kellis et al., 2003); from the Swiss-Prot (expasy.ch) and NCBI (ncbi.nlm.nih.gov) databases (Cronshaw et al., 2002); from the Wormbase (wormbase.org database); and from the *S. pombe* Gene Data Bank (genedb.org). For simplicity, the nup FG domains were defined as the largest contiguous sequence of aa containing FG motifs separated by <100 aa and including 10 additional aa flanking the first and last FG motif.

Supplemental Data

Supplemental Data include six figures and two tables and can be found with this article online at http://www.cell.com/cgi/content/full/129/1/83/DC1/.

ACKNOWLEDGMENTS

We thank D. Kellogg for Nap1 antibodies, V. Citovsky for a mLexA-Gal4AD construct, S. Wente for Cre-Lox plasmids and protocols,

S. Hanes for pSH18-34, S. Lindquist for a Sup35NM-YFP plasmid, D. Gilchrist for Kap95-YFP, J. Wright and J. Yamada for Nup100 (aa 300–400) constructs, and D. Denning for helpful discussions and bioinformatics data.

Received: June 20, 2006
Revised: November 23, 2006
Accepted: January 24, 2007
Published: April 5, 2007

REFERENCES

Allen, N.P., Huang, L., Burlingame, A., and Rexach, M.F. (2001). Proteomic analysis of nucleoporin interacting proteins. J. Biol. Chem. *276*, 29268–29274.

Allen, N.P., Patel, S.S., Huang, L., Chalkley, R.J., Burlingame, A., Lutzmann, M., Hurt, E.C., and Rexach, M. (2002). Deciphering networks of protein interactions at the nuclear pore complex. Mol. Cell. Proteomics *1*, 930–946.

Cronshaw, J.M., Krutchinsky, A.N., Zhang, W., Chait, B.T., and Matunis, M.J. (2002). Proteomic analysis of the mammalian nuclear pore complex. J. Cell Biol. *158*, 915–927.

De Souza, C.P., Osmani, A.H., Hashmi, S.B., and Osmani, S.A. (2004). Partial nuclear pore complex disassembly during closed mitosis in Aspergillus nidulans. Curr. Biol. *14*, 1973–1984.

Denning, D., Mykytka, B., Allen, N.P., Huang, L., Al, B., and Rexach, M. (2001). The nucleoporin Nup60p functions as a Gsp1p-GTP-sensitive tether for Nup2p at the nuclear pore complex. J. Cell Biol. *154*, 937–950.

Denning, D.P., Patel, S.S., Uversky, V., Fink, A.L., and Rexach, M. (2003). Disorder in the nuclear pore complex: the FG repeat regions of nucleoporins are natively unfolded. Proc. Natl. Acad. Sci. USA *100*, 2450–2455.

Denning, D.P., and Rexach, M.F. (2007). Rapid evolution exposes the boundaries of domain structure and function in natively unfolded FG nucleoporins. Mol. Cell Proteomics *6*, 272–282.

Eaglestone, S.S., Ruddock, L.W., Cox, B.S., and Tuite, M.F. (2000). Guanidine hydrochloride blocks a critical step in the propagation of the prion-like determinant [PSI(+)] of Saccharomyces cerevisiae. Proc. Natl. Acad. Sci. USA *97*, 240–244.

Feldherr, C.M., and Akin, D. (1997). The location of the transport gate in the nuclear pore complex. J. Cell Sci. *110*, 3065–3070.

Frey, S., Richter, R.P., and Gorlich, D. (2006). FG-rich repeats of nuclear pore proteins form a three-dimensional meshwork with hydrogel-like properties. Science *314*, 815–817.

Gillen, K.M., Pausch, M., and Dohlman, H.G. (1998). N-terminal domain of Gpa1 (G protein alpha) subunit) is sufficient for plasma membrane targeting in yeast Saccharomyces cerevisiae. J. Cell Sci. *111*, 3235–3244.

Kellis, M., Patterson, N., Endrizzi, M., Birren, B., and Lander, E.S. (2003). Sequencing and comparison of yeast species to identify genes and regulatory elements. Nature *423*, 241–254.

Kenna, M.A., Petranka, J.G., Reilly, J.L., and Davis, L.I. (1996). Yeast N1e3p/Nup170p is required for normal stoichiometry of FG nucleoporins within the nuclear pore complex. Mol. Cell. Biol. *16*, 2025–2036.

Lim, R.Y., Huang, N.P., Koser, J., Deng, J., Lau, K.H., Schwarz-Herion, K., Fahrenkrog, B., and Aebi, U. (2006). Flexible phenylalanine-glycine nucleoporins as entropic barriers to nucleocytoplasmic transport. Proc. Natl. Acad. Sci. USA *103*, 9512–9517.

Mohana-Borges, R., Pacheco, A.B., Sousa, F.J., Foguel, D., Almeida, D.F., and Silva, J.L. (2000). LexA repressor forms stable dimers in solution. The role of specific dna in tightening protein-protein interactions. J. Biol. Chem. *275*, 4708–4712.

Rhee, Y., Gurel, F., Gafni, Y., Dingwall, C., and Citovsky, V. (2000). A genetic system for detection of protein nuclear import and export. Nat. Biotechnol. *18*, 433–437.

Ribbeck, K., and Gorlich, D. (2001). Kinetic analysis of translocation through nuclear pore complexes. EMBO J. *20*, 1320–1330.

Ribbeck, K., and Gorlich, D. (2002). The permeability barrier of nuclear pore complexes appears to operate via hydrophobic exclusion. EMBO J. *21*, 2664–2671.

Rout, M.P., Aitchison, J.D., Suprapto, A., Hjertaas, K., Zhao, Y., and Chait, B.T. (2000). The yeast nuclear pore complex: composition, architecture, and transport mechanism. J. Cell Biol. *148*, 635–651.

Serio, T.R., Cashikar, A.G., Kowal, A.S., Sawicki, G.J., Moslehi, J.J., Serpell, L., Arnsdorf, M.F., and Lindquist, S.L. (2000). Nucleated conformational conversion and the replication of conformational information by a prion determinant. Science *289*, 1317–1321.

Shulga, N., and Goldfarb, D.S. (2003). Binding dynamics of structural nucleoporins govern nuclear pore complex permeability and may mediate channel gating. Mol. Cell. Biol. *23*, 534–542.

Shulga, N., Mosammaparast, N., Wozniak, R., and Goldfarb, D.S. (2000). Yeast nucleoporins involved in passive nuclear envelope permeability. J. Cell Biol. *149*, 1027–1038.

Strawn, L.A., Shen, T., Shulga, N., Goldfarb, D.S., and Wente, S.R. (2004). Minimal nuclear pore complexes define FG repeat domains essential for transport. Nat. Cell Biol. *6*, 197–206.

Tran, E.J., and Wente, S.R. (2006). Dynamic nuclear pore complexes: life on the edge. Cell *125*, 1041–1053.

Vernet, T., Dignard, D., and Thomas, D.Y. (1987). A family of yeast expression vectors containing the phage f1 intergenic region. Gene *52*, 225–233.

Weis, K. (2003). Regulating access to the genome: nucleocytoplasmic transport throughout the cell cycle. Cell *112*, 441–451.

Yang, M., Wu, Z., and Fields, S. (1995). Protein-peptide interactions analyzed with the yeast two-hybrid system. Nucleic Acids Res. *23*, 1152–1156.

Yang, Q., Rout, M.P., and Akey, C.W. (1998). Three-dimensional architecture of the isolated yeast nuclear pore complex: functional and evolutionary implications. Mol. Cell *1*, 223–234.